IRAQI JOURNAL OF APPLIED PHYSICS
Vol. 22, No. 2, April-June 2026, pp. 196-204

Aneed M. Lafta [1]
Dunia K. Mahdi [2*]
Khalid H. Razeg [3]
Inaam M. Abdulmajeed [2]
Baha T. Chiad [2]
Amera G. Baker [4]
Ahmad A. Hasan [2]

[1] Ministry of Education, General Directorate of Education of Salah-Alden, Salah-Alden Province, IRAQ
[2] Department of Physics, College of Science, University of Baghdad, Baghdad, IRAQ
[3] Al Hathara University College, Tikrit, IRAQ
[4] Department of Physics, Faculty of Science and Health, Koya University, Koya 44023, Kurdistan Region, IRAQ
* Corresponding author email: dunia.kamil@sc.uobaghdad.edu.iq

Simulated Body Fluid Immersion Time Effects on Sol-Gel Phosphate Glass-Ceramic Structure

A SiO_2-CaO-Na_2O-P_2O_5 bioactive glass-ceramic was successfully synthesized via sol-gel method using sodium metasilicate. XRD analysis for immersed simulated body fluid (SBF) samples revealed the presence of predominant peaks corresponding to poly-crystalline Hydroxyl-apatite $Ca_{10}(PO_4)6(OH)_2$ with hexagonal structure as well as complete transformation of biphasic structure $Na_2Ca_2Si_3O_9$ and $Na_6Ca_2P_2Si_3O_9$ phases for standard sample. Remarkably, HAp nucleation occurred within 7 days. The grain size increased with immersion time, while the transformation of initial flake-like $Na_2Ca_2Si_3O_9$ structure into filamentous HAp was revealed resembling natural bone. Elemental analysis showed increasing Ca/P content and incorporation of Mg/K/Cl ions with Na^+ release. FTIR confirmed HAp formation through intensified P-O bands and diminished Si-O-Si vibrations. These results demonstrate the material's excellent bioactivity and strong potential for tissue engineering applications

Keyword: Bioactive Glass, Sol-gel, Crystalline, Sodium Metasilicate, Hydroxyapatite
Received: 27 May 2025; Revised: 8 September; Accepted: 15 September 2025

1. Introduction

Over the past few decades, bioactive glasses have revolutionized the functionality of biomaterials, transforming them from bioinert substances to bioactive agents capable of eliciting strong biological responses upon implantation in the human body [1,2]. A material is classified as bioactive when it can form stable chemical bonds with both soft and hard tissues through such responses [3]. Due to their excellent biocompatibility, silica-based glasses have attracted significant attention as second-generation biomaterials for the treatment of bone defects and soft tissue injuries [4-6]. The dissolution products of bioactive glasses have been shown to upregulate gene expression associated with osteogenesis, thereby enhancing bone regeneration more effectively than traditional inorganic ceramics such as hydroxyapatite [7-9]. However, when the silica content exceeds 60 wt.% in the glass composition, the bioactive bonding capability to tissues tends to diminish [10]. Conversely, increasing the CaO content in bioactive glasses has been correlated with enhanced bioactivity, as calcium ion release plays a crucial role in initiating chemical bonding with biological tissues [11]. Despite their advantages, implantable biomaterials carry a risk of bacterial colonization, which can lead to failure of the implant. This is especially pertinent in dental applications, where microbial activity associated with periodontal disease is a common cause of implant failure [4,5]. Therefore, continued investigation into alternative materials with improved biological responses and antibacterial properties remains critical [12]. The ionic dissolution products of bioactive glasses also contribute to enhanced osteogenic activity, highlighting their therapeutic potential [7,13]. Among the fabrication techniques, the sol-gel method offers significant advantages over conventional melt-quenching, including better compositional control, higher purity, and enhanced homogeneity [14,15]. The development of quaternary bioactive glasses with a SiO_2-CaO-Na_2O-P_2O_5 composition is well-established, traditionally utilizing alkoxysilane precursors such as tetraethyl orthosilicate (TEOS) and tetramethyl orthosilicate (TMOS) [16,17]. However, the high cost and hazardous nature of these precursors pose limitations for large-scale production [18,19]. In contrast, advantages of sodium metasilicate in bioactive glass synthesis were manifest by accelerates sol-gel processing by reducing gelation time (hours vs. days for TEOS), lower processing temperature avoiding organic residues that could compromise bioactivity. The Na^+ ions in metasilicate act as network modifiers that the enhanced bioactivity by accelerates hydroxyapatite formation (confirmed by in vitro SBF tests), reduces phase separation risks compared to TEOS-derived gels, yielding more uniform pore structures critical for

 © ALL RIGHTS RESERVED

scaffold applications. Finally, sodium metasilicate (Na_2SiO_3) is cheaper and more industrially scalable [27-29][20-22], with regarding that the high sodium content may require optimization to control dissolution rates for specific applications.

In this context, the present study aims to synthesize a sodium-containing quaternary bioactive glass-ceramic using sodium metasilicate as an economical and safer silica source. The bioactivity and structural integrity of the developed glass-ceramic are evaluated employing atomic force microscopy (AFM) and scanning electron microscopy (SEM) to investigate surface morphology and grain structure over time. Elemental analysis is performed to monitor the incorporation and distribution of calcium and phosphorus, thereby assessing compositional changes with time immersion in simulated body fluid (SBF). Thus, it can be determine its potential for application as a scaffold in tissue engineering.

2. Experimental Part

The starting materials are aquatic sodium metasilicate ($Na_2SiO_35H_2O$), nitric acid (HNO_3, from Fluka, Germany), phosphorus pentoxide (P_2O_5 supplied by BDH Laboratory) and calcium nitrate tetrahydrate ($Ca_2(NO_3)_2.4H_2O$, LOBA, 98%) were equipped for prepared samples.

Using the sol-gel method, bioactive glass with the weight percentage composition of $50SiO_2{:}25Na_2O{:}21CaO{:}4P_2O_5$ was prepared using the following protocol. To get a clear solution, 7.5 g from $Na_2SiO_3.5H_2O$ was mixed with 22.5 ml of deionized water in a beaker using a magnetic stirrer, then, 3.75 ml of ethanol was added. To allow for full hydrolysis, 2M of HNO_3 drop wise was added to the stirred mixture process, stirring was maintained for an hour. P_2O_5 (0.75 g) and $Ca(NO_3)2{\bullet}4H_2O$ (6.15 g) were added one by one with taking into account that each component gives 45 minutes to react properly while stirrer being continuously. The mixture has been agitated for an hour to achieve the gel phase. The resulting gel was aged at room temperature for 5 days, then dried at 60°C using an oven for 72 hours to obtained the monolith phase which was further heat treated at 200°C for 40 hours. The solid monolith was grinded by a mortar to get a soft powder, then, 1 g was compressed to produce a pellet (10 mm in diameter with 4 mm in thickness) using a hydraulic piston with load of 3 tons and time loading of 2 minutes. The pellets have been subjected to circle thermally heat treated procedure at different temperatures and time as follows, 600°C for 5 hours, 800°C for 3 hours, and 900°C for 1 hour.

To simulate in vitro apatite formation on bioactive materials, simulated body fluid (SBF) was prepared to mimic the inorganic ion concentrations of human extracellular fluid. The ionic components listed in Table 1 were dissolved in 1 liter of deionized water, and the solution's pH was adjusted to 7.4 using tris (hydroxyethyl) aminomethane ($((CH_2OH)_3CNH_2)$) and hydrochloric acid (HCl). This solution is commonly referred to as SBF or Kokubo solution. It is widely used not only for evaluating the in vitro bioactivity of synthetic materials but also for facilitating apatite layer deposition under biomimetic conditions.

Table (1) Ionic concentrations (mM) of the prepared SBF with those of human blood plasma [23]

Elements	Na^+	K^+	Mg^{2+}	Ca^{2+}	Cl^{1-}	HCO_3	HPO_4^{-2}	SO_4^{-2}
Plasma	142.0	5.0	1.5	2.5	103.0	27.0	1.0	0.5
SBF	142.0	5.0	1.5	2.5	147.8	42	1.0	0.5

Monolithic glass-ceramic disks samples (10×4 mm) were immersed in SBF at a concentration of 0.01 g/mL in sterilized plastic containers, pre-cleaned with HCl and deionized water. The containers were placed in a thermostatically controlled incubator maintained at 37°C. The pH meter of SBF solutions were stabilized at pH of 7.4, which was maintained constant during the experiment, using Hanna, HI96107 digital meter over 7, 14, and 21 immersion days.

At each time interval, the samples were removed from the SBF, gently rinsed with ethanol followed by deionized water, and then dried at ambient conditions in a desiccator (100°C for 2 hours). The dried specimens were analyzed using X-ray diffraction (XRD), scanning electron microscopy (SEM), energy-dispersive x-ray spectroscopy (EDS), atomic force microscopy (AFM), and Fourier-transform infrared spectroscopy (FTIR) to confirm the formation of an apatite layer on the glass surface.

3. Results and Discussion

The XRD patterns of ceramic glass pellets without and with immersed at different time in simulated body fluid (SBF) was shown in Fig. (1). This figure shows that the immersed samples reveal the presence of the predominant peaks corresponding to poly-crystalline Hydroxyl-apatite $Ca_{10}(PO_4)6(OH)_2$ with hexagonal structure which identical with JCPDS card 96-901-1095. The parent phases (Mono $Na_6Ca_2P_2Si_3O_9$ and Hex $Na_6Ca_2Si_3O_9$) were disappeared from XRD patterns indicating to hydroxyl-apatite phase transformation cover all samples surfaces which has high diffraction structure factor. Disappeared phases can be attributed to the formation of new bonds between ingredients and formation of bone regeneration structure (hydroxyl-apatite). The peaks appeared with broad feature especially for the preferred orientation along (112), i.e., the crystalline with small size. Increasing the immersing time from 1 week to 3 weeks cause to enhance the crystallinity, so increase the peaks intensities of the bioactive glass. The most intense peaks match well the conventional PDF file 96-

 © ALL RIGHTS RESERVED

901-1095, suggesting that the $Na_2Ca_2Si_3O_9$ crystalline phase had formed. In vitro bioactivity evaluation in simulated body fluid (SBF) for a maximum of 21 days indicated the formation of hydroxyapatite on the sample surface.

The diffraction peaks of glass ceramic samples immersed in different times was listed in table (2), which also contains Bragg's angle (2θ), full-width at half maximum (FWHM), experimental inter-planar spacing (calculated using Bragg low) compared with standard ones, Scherrer's equation was used to calculated the crystallite size and the corresponding planes. The average crystallite size increase from 8.4 to 10.5 nm with increasing the immersing time from 1 week to 3 weeks due to increasing the deposited apatite substance, consequently, particles agglomeration. The reason to emphasis this specific angle (2θ =47.42°) that it is represented to the bioactive or apatite layer. The computation crystallite size that obtained from x-ray pattern giving more interesting information which support the claim that the increasing immersion time produce small crystallite size and enhanced crystallinity over time.

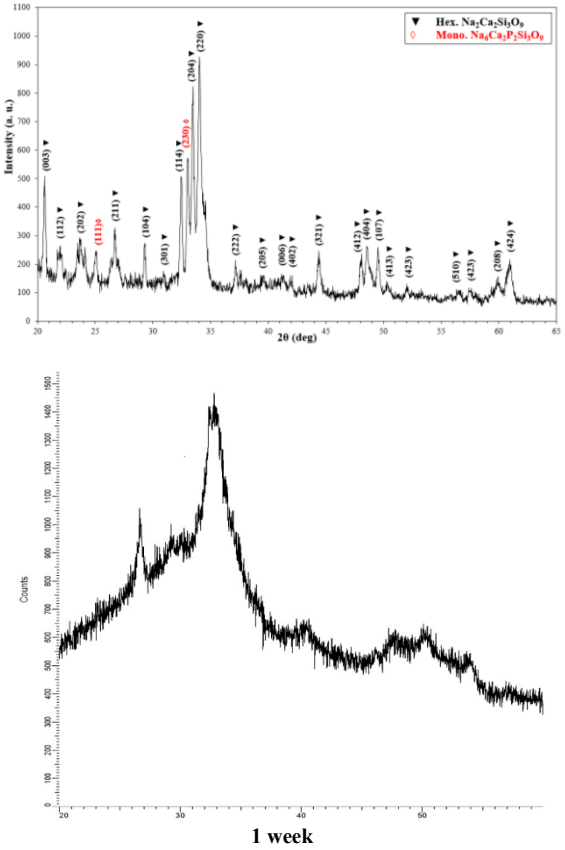

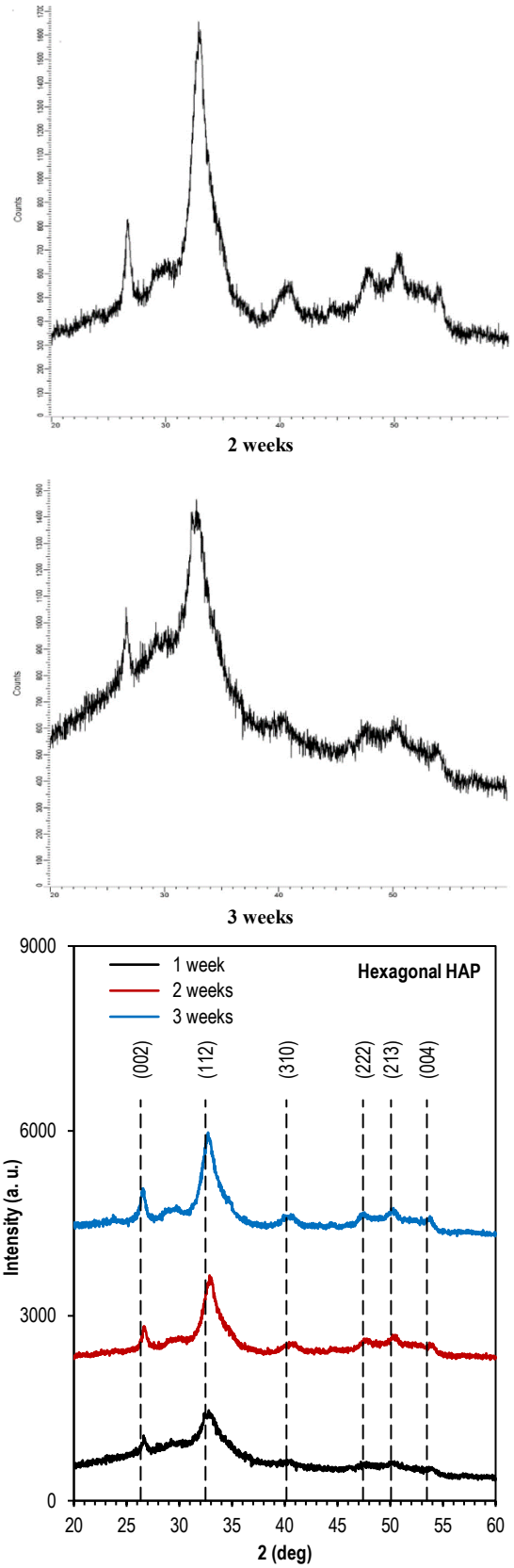

Fig. (1) XRD patterns for standard and immersed glass ceramic in SBF at different interval time (a) 1 week, (b) 2 weeks, (c) 3 weeks

 © ALL RIGHTS RESERVED

The surface topography and the distribution of granulates for biomaterial before and after immersion in SBF in different times was illustrated in the AFM images as shown in Fig. (2). The average grain size increase with increasing immersing time due to agglomerated and deposited of apatite layer.

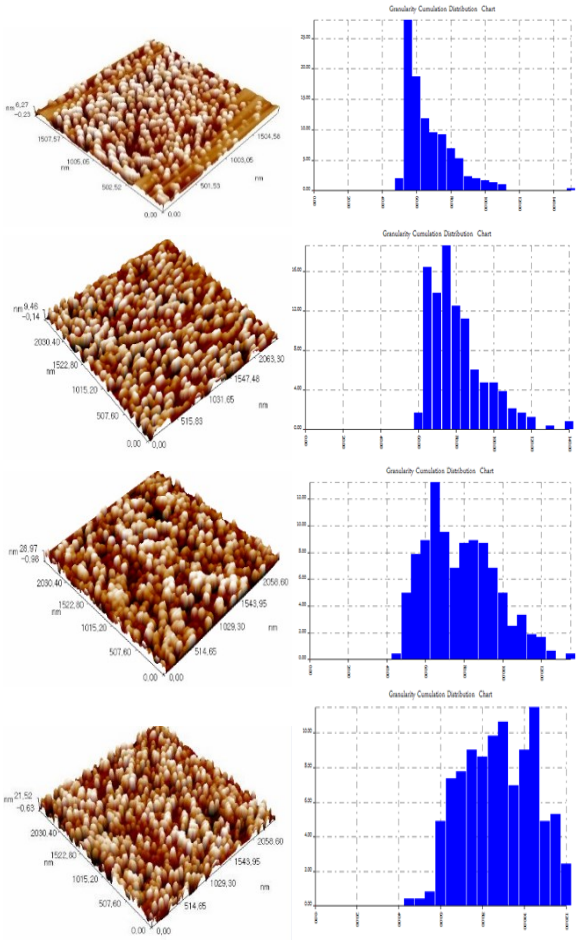

Fig. (2) 3D AFM images illustrating the granularity accumulation distribution for biomaterial before and after immersing in SBF in different times

The average diameter (nm) for the slandered sample is 64.94 nm, particle size was increased to 78.4 nm for the first week which is possible to aggregation or initial mineral deposition, more increasing in the third week to 85.14 (31%↑ from standard) → likely hydroxyapatite (HA) layer formation.The increase in diameter over time suggests surface mineralization (e.g., Ca-P deposition), consistent with bioactive behavior.

Baseline RMS Roughness ($R_{q,n}$) is 7.32 nm, early SBF interaction (ion exchange) was observed in the first week to be 8.63 nm, surface smoothing in the second week (2.83 → 61%↓) maybe due to silica gel formation, recovery roughness 6.45 produce HA crystallization creating micro-scale features. Roughness rebounds due to HA crystallization, creating a textured surface favorable for cell adhesion, Diameter growth matches EDX data showing Ca/P rise HA formation and roughness dip correlates with FTIR's Si–O–Si degradation (Week 2).

Table (3) AFM parameters for biomaterial before and after immersing in SBF at different times

Immersing time in SBF	Average Diameter (nm)	RMS roughness (nm)	Average Roughness (nm)
Standard	64.94	7.32	7.11
1 week	78.42	8.63	7.46
2 week	75.60	2.83	2.47
3 week	85.14	6.45	5.61

SEM images of the glass-ceramic sample at magnifications of 4000x, 20000x, and 35000x are presented in Fig. (3a). The micrographs reveal flake-like structures associated with the glassy $Na_2Ca_2Si_3O_9$ phase. These flakes, ranging from 0.58 to 0.9 µm in diameter, aggregate uniformly across the surface. In addition, numerous nanorods are observed, dispersed within surface pores. The sample also exhibits elongated, filamentous structures with polygonal cross-sections and thicknesses between 47 and 187 nm. These features indicate the formation of an appetite phase, consistent with findings from previous studies [25][23].

After one week of immersion in simulated body fluid (SBF), the surface becomes coated with branched, needle-like hydroxyapatite crystals, and the pore size decreases significantly. As shown in Fig. (3b), this nanostructured hydroxyapatite layer demonstrates the in vitro bioactivity of the bio-glass. At higher magnification, the surface appears densely populated with fine hydroxyapatite needles. These nanocrystals are similar to those found in human bone and are believed to enhance tissue formation, cellular adhesion, and proliferation.

Figures (3a-d) display the evolution of the surface morphology at different immersion times. With extended immersion (2 and 3 weeks), belt-like structures form, indicating increased thickness of the apatite layer (Figs. 3c and 3d). These observations align with XRD results. Notably, the tips of the hydroxyapatite needles exhibit bright regions suggestive of active growth zones. This implies that prolonged immersion promotes the elongation of these structures elemental analysis of the unimmersed sample (Fig. 3a) shows prominent peaks for Na, Ca, Si, and O, confirming the glass matrix composition, in addition to small K_α and K_β peaks for phosphorus (P) indicate residual phosphate, while trace carbon (C) suggests the partial presence of organic residues such as ethanol.

Elemental quantification was conducted using EDS software, based on K_α peak intensities and atomic transition probabilities (table 4). The atomic ratios closely match the stoichiometry of $Na_2Ca_2Si_3O_9$.

Following immersion in SBF for more time (2 and 3 weeks), phosphorus peaks intensify and new peaks corresponding to Mg, K, and Cl appear, indicating the formation of a hydroxyapatite layer derived from the

 © ALL RIGHTS RESERVED

SBF components (Figs. 3b-d). Ion exchange process is very clear in this section due to increasing in P and Ca ions post-immersion in addition to Na, Si and O, these elements have an effective and major role in apatite texture formation which gives great importance to tis research.

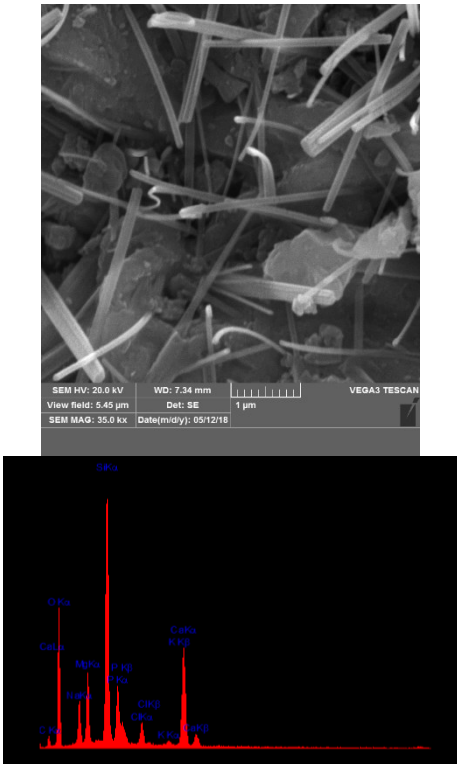

(a)

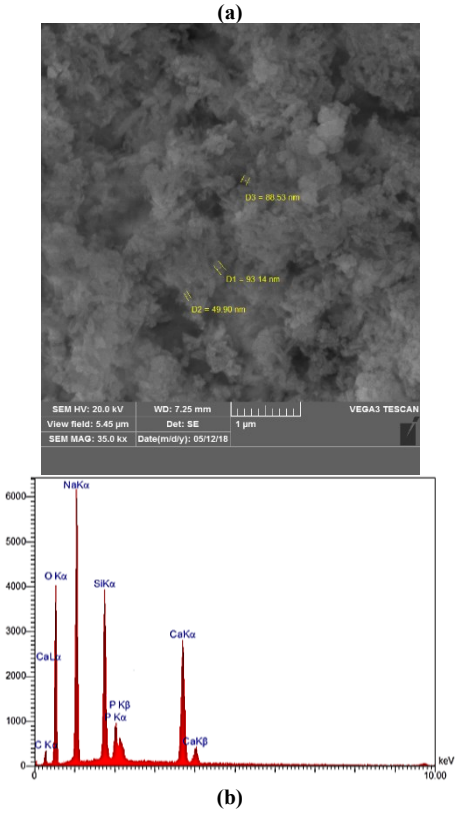

(b)

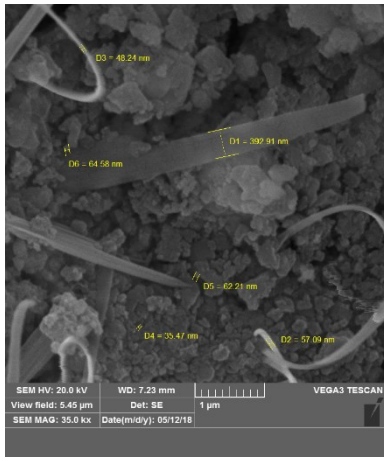

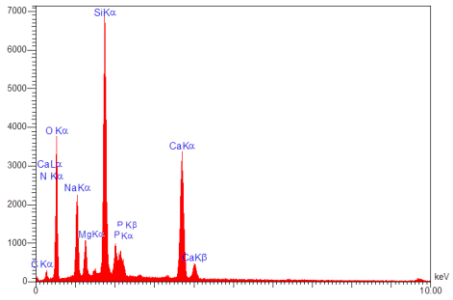

(c)

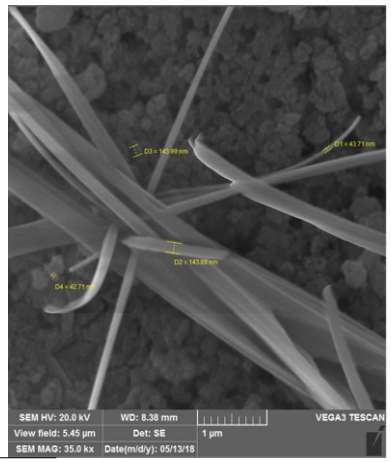

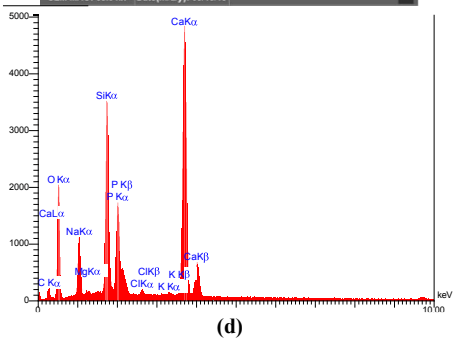

(d)

Fig. (3) SEM images and EDX spectra for (a) prepared glass ceramic before immersed in SBF, (b) prepared biomaterial glass ceramic immersed 1 week, (c) prepared biomaterial glass ceramic immersed for 2 week in SBF, and (d) prepared biomaterial glass ceramic immersed in 3 week in SBF

 © ALL RIGHTS RESERVED

A significant increase in Ca content (from 9.76 wt.% to 22.65 wt.% by 3 weeks) and P content (0.61 wt.% to 5.36 wt.%) after immersion indicates phosphate ion incorporation from SBF, supporting hydroxyapatite (HA) nucleation suggests the active deposition of calcium phosphate phases. The rise correlates with the formation of an appetite layer. The fluctuation at 2 weeks may reflect transient precursor phases (e.g., amorphous calcium phosphate). Leaching of magnesium and sodium which subsequent decrease (4.68 wt.% to 0.26 wt.%) and (19.83 wt.% to 5.32 wt.%) that implies incorporation into the apatite layer or reabsorption into the fluid as well as, Na suggests ion exchange with H^+/H_3O^+ from SBF for surface activation and Si-OH group formation, which aids HA nucleation. The initial increase of silica from (7.66 wt.% to 13.23 wt.% at 1 week) releasing silicic acid to promote HA formation.

The EDS data validate the material's bioactivity, evidenced by HA layer formation and ion exchange dynamics. The progressive Ca/P increase and Na/Mg trends mirror in vivo bioactive behavior, promising for bone regeneration applications. Table (4) summarizes the elemental composition before and after immersion.

Table (4) EDS data and elemental composition of the prepared samples over immersion time (wt.%)

Element	Standard	1 week	2 weeks	3 weeks
C	11.80	13.64	6.56	8.90
O	50.31	48.95	54.92	48.26
Na	19.83	3.92	7.32	5.32
Mg	–	4.68	2.87	0.26
Si	7.66	13.23	12.49	8.64
P	0.61	4.10	3.52	5.36
Cl	–	1.71	0.44	0.36
K	–	0.43	0.30	0.25
Ca	9.76	9.33	11.54	22.65

Figure (4) illustrates the variation in elemental percentages over time. A marked increase in P and Ca content is observed with immersion, alongside a notable decrease in Na, attributed to ion exchange and Na^+ release into the solution - a phenomenon reported in previous studies [23][24].

The chart illustrates the changes in the atomic percentage (at.%) of various elements (C, Na, Mg, K, Si, P, Cl, Ca) in Sample A over time (0 to 3 weeks) as it is immersed in simulated body fluid (SBF). These changes reveal the material's bioactive behavior, particularly its ability to form a bone-like apatite layer, which is crucial for bone regeneration applications.

The relation between the existing ions can be interpreted as follow:

Calcium and phosphorus rises gradually by 3 weeks (~22 at.%, ~3.5 at.%, respectively), indicating active deposition of calcium from SBF onto the material's surface and pairing of P with Ca to form calcium phosphate phases (e.g., amorphous precursors → crystalline hydroxyapatite). The growing Ca/P ratio (closer to 1.67, the ideal for hydroxyapatite) confirms bioactive potential. Sodium drops dramatically (from ~16 at.% to ~5 at.%) due to ion exchange with SBF (Na^+ replaced by H_3O^+). This creates a reactive surface for apatite nucleation.

Magnesium appears after immersion (peaks at ~3.5 at.%), then declines. This suggests Mg from SBF is either incorporated into the apatite layer, or reabsorbed into solution as crystallization progresses.

The presence of hydroxyapatite was further confirmed by FTIR spectroscopy (Fig. 5). Spectra obtained before and after immersion in SBF for 7, 14, and 21 days reveal characteristic peaks associated with hydroxyapatite formation: P–O bending in crystalline phosphate P-O (568-604 cm^{-1}) and non-bridging PO_2 groups (1420-1490 cm^{-1}). Upon immersion, increased intensity of P–O vibrational bands indicates the growth of an amorphous calcium phosphate layer. Furthermore, Si–O–Si stretching and bending modes, observed at 875-918 cm^{-1} and 425-497 cm^{-1} respectively, become more defined with immersion, suggesting enhanced crystallization. A decrease in Si–O–Si peak intensity near 918 cm^{-1} after 3 weeks suggests the presence of a thicker hydroxyapatite layer. These findings are consistent with literature reports [26][25].

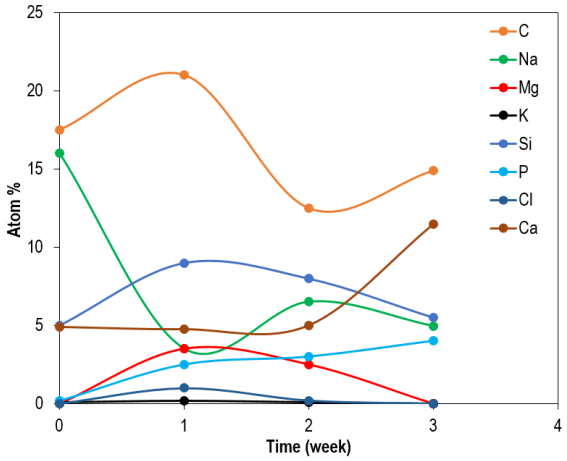

Fig. (4) The variation of elemental atomic percentages (at.%) for samples over immersion time in SBF

3.1 Glass-Ceramic Degradation and Hydroxyapatite Formation

To complement the EDS data, FTIR spectra were analyzed for prepared samples after immersion in SBF for 0, 1, 2, and 3 weeks. The remarkable bands assignments and their modification can be detailed below, with a focus on P–O (phosphate) and Si–O–Si (silicate) vibrations. The phosphate (P–O) bands containing characteristic peaks confirming the formation of hydroxyapatite were observed. The ν_3 mode (PO_4^{3-} stretching) was absent in the first week (no phosphate in original material). The broad band at

 © ALL RIGHTS RESERVED

1040-1100 cm^{-1} is ascribed to amorphous calcium phosphate, ACP (Week 1). From week 2-3, a sharp peak at 1032 cm^{-1} attributed to the crystalline hydroxyapatite (HA) and splits into 1090 cm^{-1} (ν_3 asymmetric stretch of PO_4^{3+} bending). Bands at 560-600 cm^{-1} (doubly degenerate bend) and 602 cm^{-1} (ν_4 bend) confirm HA crystallization. So, the shift from broad to sharp peaks indicates ACP→HA transformation and splitting of ν_3 (1032/1090 cm^{-1}) and ν_4 (560/602 cm^{-1}) is definitive for crystalline HA (JCPDS card 09-0432).

The strong band at ~1050 cm^{-1} (bridging oxygen in SiO_4 network) in standard sample is related to Si–O–Si stretch. For the 1-2 Week, shifts to ~950 cm^{-1} (non-bridging $Si–O^-$ groups) are due to Na^+ leaching. Further weakens, with a new band at ~800 cm^{-1} (Si–OH bending, silica gel dissolution (Si–OH stretching) Broad band at ~3450 cm^{-1} (silanol groups, Si–OH), confirms gel formation. The Si–OH growth (at 3450 cm^{-1}) correlates with EDS's Si peak (Week 1-2), supporting silica gel's role in HA nucleation. Weak band at 1415-1450 cm^{-1} (ν_3 CO_3^{2-}) is possibly from surface adsorption of CO_2 from air carbonated HA (CO_3^{2-} substituting PO_4^{3-}), and affect biological apatite.

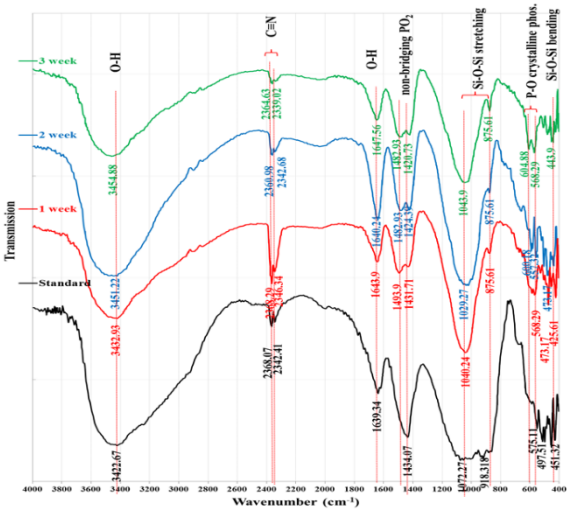

Fig. (5) FTIR spectrum for prepared glass ceramic before and after immersing in simulated body fluid at different times

Table (5) illustrates a comparison between the specific functional groups (the common peaks) in FTIR spectra of glass-ceramic biomaterial in the present work before and after immersing in simulated body fluid (SBF).

4. Conclusions

A bioactive glass-ceramic with a composition based on SiO_2–CaO–Na_2O–P_2O_5 was successfully synthesized via sol-gel method. The poly-crystalline Hydroxyl-apatite $Ca_{10}(PO_4)_6.(OH)_2$ hexagonal structure was confirmed. The parent phases (Mono $Na_6Ca_2P_2Si_3O_9$ and hex $Na_6Ca_2Si_3O_9$) were subject to hydroxyl-apatite phase transformation. The increase in particle diameter over time suggests surface mineralization (e.g., Ca-P deposition), consistent with bioactive behavior. A significant increase in Ca and P content after immersion indicates phosphate ion incorporation from SBF, supporting hydroxyapatite (HA) nucleation. Leaching of Mg and Na which subsequently decreases implies incorporation into the apatite layer or reabsorption into the fluid as well as, Na suggests ion exchange with H^+/H_3O^+ from SBF for surface activation and Si-OH group formation, which aids HA nucleation. The material's structural evolution and bioactive performance suggest strong potential for bone regeneration applications, combining the advantages of sol-gel processing with clinically relevant biological activity.

Table (5) Comparison between FTIR bands for glass ceramic before and after immersing in SBF at different times

	immersing time			
	Standard	**1 week**	**2 weeks**	**3 weeks**
Si-O-Si bending	451.32	425.61	-	443.90
	497.51	473.17	473.17	-
P-O in crystalline phosphate	575.11	568.29	557.32	568.29
	-	-	600.18	604.88
Si-O-Si stretching	918.32	875.61	875.61	875.61
	1072.27	1040.24	1029.27	1043.90
non-bridging PO_2	1434.07	1431.71	1424.39	1420.73
	-	1493.90	1482.93	1482.93
O-H	1639.34	1643.90	1640.24	1647.56
C≡N	2342.41	2346.34	2342.68	2339.02
	2368.07	2368.29	2360.98	2364.63
O-H	3422.67	3432.93	3451.22	3454.88

References

[1] P. Stoor, E. Soderling and J.I. Salonen, "Antibacterial activity of bioactive glass granules", *Acta Odontol. Scand.*, 56(3) (1998) 161-165.

[2] R.H. Hussian and D.K. Mahdi, "Investigation the Structural Influences of Silver Oxide Addition in the Bioactive Phosphate Glasses", *East Eur. J. Phys.*, 3 (2023) 321-328.

[3] L.L. Hench, R.J. Splinter and W.C. Allen, "Bonding mechanisms at the interface of ceramic prosthetic materials", *J. Biomed. Mater. Res.*, 5(6) (1971) 117-141.

[4] G. Goller et al., "Processing and characterization of bioglass reinforced hydroxyapatite composites", *Ceram. Int.*, 29(6) (2003) 721-724.

[5] L.L. Hench and J. Wilson, "Surface-Active Biomaterials", *Science*, 226(4675) (1984) 630-636.

[6] T.A. Kareem and D.K. Mahdi, "Synthesis and characterization of silver nanoparticles-doped mesoporous bioactive glass prepared by spray pyrolysis", *Eurasian Chem. Commun.*, 4(4) (2022) 330-337.

 © ALL RIGHTS RESERVED

[7] L.L. Hench, "Genetic Design of Bioactive Glass", *J. Eur. Ceram. Soc.*, 29(7) (2009) 1257-1265.
[8] S.K. Ghosh et al., "In vivo response of porous hydroxyapatite and β-tricalcium phosphate prepared by aqueous solution combustion method and comparison with bioglass scaffolds", *J. Biomed. Mater. Res. B*, 86(1) (2008) 217-227.
[9] I.M. Abdulmajeed and S.H. Ibraheem, "Preparation and Characterization of Biomaterial Powder by Sol-gel Method", *Iraqi J. Appl. Phys.*, 19(4) (2023) 71-80.
[10] R. Li, A.E. Clark and L.L. Hench, "An investigation of bioactive glass powders by sol-gel processing", *J. Appl. Biomater.*, 2(4) (1991) 231-239.
[11] G. Laudisio and F. Branda, "A DSC study of the crystallization of a sol–gel derived bioactive glass", *Thermochim. Acta*, 370(1-2) (2001) 119-124.
[12] I.D. Xynos et al., "Gene-Expression Profiling of Human Osteoblasts Following Treatment with Ionic Products of Bioglass® 45S5 Dissolution", *J. Biomed. Mater. Res.*, 55(2) (2001) 151-157.
[13] S. Sakka, **"Handbook of Sol-Gel Science and Technology: Processing, Characterization and Applications"**, Kluwer Acad. Pub. (NY, 2005).
[14] J.R. Jones, "New Trends in Bioactive Scaffolds: The Importance of Nanostructure", *J. Eur. Ceram. Soc.*, 29(7) (2009) 1275-1281.
[15] R.L. Siqueira, O. Peitl and E.D. Zanotto, "Gel-Derived SiO_2-CaO-Na_2O-P_2O_5 Bioactive Powders Synthesis and in Vitro Bioactivity", *Mater. Sci. Eng. C*, 31(5) (2011) 983-991.
[16] P. Saravanapavan et al., "Bioactivity of Gel-Glass Powders in the CaO-SiO_2 System: A Comparison with Ternary (CaO-P_2O_5-SiO_2) and Quaternary Glasses (SiO_2-CaO-P_2O_5-Na_2O)", *J. Biomed. Mater. Res. A*, 66(1) (2003) 110-119.
[17] Z. Li et al., "Comparative Study of Sol-Gel Hydrothermal and Sol-Gel Synthesis of Titania-Silica Composite Nanoparticles", *J. Solid State Chem.*, 178(5) (2005) 1395-1405.
[18] T. Kokubo and H. Takadama, "How Useful Is SBF in Predicting in Vivo Bone Bioactivity?", *Biomaterials*, 27(15) (2006) 2907-2915.
[19] Z.H.A. Al-Mothafer and I.M. Abdulmajeed, "Comparative study in use sodium silicate instead of NH_4OH as an alkaline basic catalyst to gelation unmodified silica aerogel based on tetraethoxysilane (TEOS)", *J. Ovonic Res.*, 17(4) (2021) 373-382.
[20] G. Kaur, O.P. Pandey and K. Singh, "Rapid sol-gel synthesis of bioactive glasses using sodium metasilicate as an alternative precursor", *Mater. Sci. Eng. C*, 108 (2020) 110429.
[21] D. Zhang, M. Hupa and L. Hupa, "Influence of sodium and calcium content on the in vitro bioactivity of glasses", *Ceram. Int.*, 47(12) (2021) 17380-17388.
[22] R. Li, A.E. Clark and L.L. Hench, "An economic evaluation of bioactive glass production methods", *J. Mater. Chem. B*, 11 (2023) 3256-3269.
[23] S. Zhang, **"Hydroxyapatite Coatings for Biomedical Applications"**, 1st ed., CRC Press (2018).
[24] D.C. Clupper et al., "Bioactivity of Tape Cast and Sintered Glass-Ceramics in Simulated Body Fluid", *Biomaterials*, 23(12) (2002) 2599-2606.
[25] Z.S. Sadeq, S.M. Alshrefi and D.K. Mahdi, "Study the nonlinear behavior of MWCNTs and ZnO/Se/MWCNTs", *AIP Conf. Proc.*, 2123(1) (2019) 020089.
[26] H. Mohamad et al., "Effects of alumina (Al_2O_3) addition on mechanical property of fabricated melt-derived bioactive glass", *AIP Conf. Proc.*, 1791(1) (2016).

 © ALL RIGHTS RESERVED

XRD parameters for standard and immersed glass ceramic

2θ (Deg.)	FWHM (Deg.)	d_{hkl} Exp.(Å)	C.S (nm)	d_{hkl} Std.(Å)	hkl	Phase	card No.
20.6256	0.2502	4.3028	32.3	4.3893	(003)	Hex.	96-200-3537
22.0019	0.4588	4.0367	17.6	4.0962	(112)	Hex.	96-200-3537
23.7118	0.6256	3.7493	13.0	3.7326	(202)	Hex.	96-200-3537
25.0880	0.3337	3.5467	24.4	3.5527	(130)	Mono.	96-901-1878
26.7146	0.5839	3.3343	14.0	3.3148	(211)	Hex.	96-200-3537
29.3003	0.2502	3.0457	32.8	3.0942	(104)	Hex.	96-200-3537
30.9268	0.2085	2.8891	39.5	2.9442	(301)	Hex.	96-200-3537
32.4699	0.2502	2.7552	33.1	2.7863	(114)	Hex.	96-200-3537
33.0120	0.2503	2.7112	33.1	2.7162	(230)	Hex.	96-901-1878
33.4708	0.2502	2.6751	33.2	2.6633	(204)	Hex.	96-200-3537
34.0547	0.2919	2.6306	28.5	2.6160	(220)	Hex.	96-200-3537
37.1826	0.2502	2.4161	33.5	2.4311	(222)	Hex.	96-200-3537
39.4764	0.3753	2.2809	22.5	2.2769	(205)	Hex.	96-200-3537
41.2280	0.3753	2.1879	22.6	2.1947	(006)	Hex.	96-200-3537
41.9370	0.4170	2.1526	20.4	2.1422	(402)	Hex.	96-200-3537
44.3976	0.4170	2.0388	20.6	2.0535	(321)	Hex.	96-200-3537
48.1094	0.2920	1.8898	29.8	1.8939	(412)	Hex.	96-200-3537
48.5681	0.3754	1.8730	23.2	1.8663	(404)	Hex.	96-200-3537
49.5273	0.2920	1.8390	30.0	1.8419	(107)	Hex.	96-200-3537
50.2780	0.4171	1.8133	21.0	1.8030	(413)	Hex.	96-200-3537
52.0297	0.3754	1.7563	23.5	1.7578	(324)	Hex.	96-200-3537
56.5338	0.4588	1.6265	19.7	1.6276	(510)	Hex.	96-200-3537
57.6182	0.4171	1.5985	21.7	1.5954	(423)	Hex.	96-200-3537
59.9120	0.4171	1.5427	22.0	1.5471	(208)	Hex.	96-200-3537
60.9546	0.4170	1.5187	22.1	1.5193	(424)	Hex.	96-200-3537

Table (2) Structural parameters for glass ceramic immersed at different time in SBF

immersing time	2θ (Deg.)	FWHM (Deg.)	d_{hkl} Exp.(Å)	C.S (nm)	d_{hkl} Std.(Å)	hkl	card No.
	26.3329	0.6054	3.3818	13.5	3.4395	(002)	96-901-1095
	32.4796	1.4901	2.7544	5.6	2.7781	(112)	96-901-1095
1 week	40.1630	1.1176	2.2434	7.6	2.2636	(310)	96-901-1095
	47.4272	1.0244	1.9154	8.5	1.9437	(222)	96-901-1095
	50.0815	1.5832	1.8199	5.5	1.8403	(213)	96-901-1095
	53.4808	0.9313	1.7120	9.6	1.7198	(004)	96-901-1095
	26.4261	0.5123	3.3700	15.9	3.4395	(002)	96-901-1095
	32.6193	1.4901	2.7430	5.6	2.7781	(112)	96-901-1095
2 week	40.3958	1.4435	2.2310	5.9	2.2636	(310)	96-901-1095
	47.4272	0.9779	1.9154	8.9	1.9437	(222)	96-901-1095
	50.0815	0.7916	1.8199	11.1	1.8403	(213)	96-901-1095
	53.6205	0.6519	1.7078	13.7	1.7198	(004)	96-901-1095
	26.2864	0.5588	3.3876	14.6	3.4395	(002)	96-901-1095
	32.4331	1.3969	2.7583	5.9	2.7781	(112)	96-901-1095
3 week	40.2095	1.3970	2.2410	6.1	2.2636	(310)	96-901-1095
	47.2875	0.8382	1.9207	10.3	1.9437	(222)	96-901-1095
	49.9418	0.8848	1.8247	9.9	1.8403	(213)	96-901-1095
	53.5274	0.5588	1.7106	15.9	1.7198	(004)	96-901-1095

 © ALL RIGHTS RESERVED